Acta Mech 227, 2011–2024 (2016)
DOI 10.1007/s00707-016-1604-7

ORIGINAL PAPER

M. Yu · Q. H. Fang · H. Feng · Y. W. Liu

Effect of special rotational deformation on dislocation emission from interface collinear crack tip in nanocrystalline bi-materials

Received: 22 November 2015 / Revised: 23 January 2016 / Published online: 8 April 2016

Abstract The work is devoted to investigate the interaction between the special rotational deformation and interface collinear cracks in nanocrystalline bi-materials. As an illustrative example, the effect of the disclination quadrupole produced by the special rotational deformation on the emission of lattice dislocation from a finite interfacial crack tip in nanocrystalline bi-material is explored theoretically using the complex variable method. The complex form expression of dislocation force and the critical stress intensity factors for the first edge dislocation emission under remote mode I loadings and mode II loadings are deduced. And the influences of material properties, grain size, disclination strength, disclination location and orientation, special rotational deformation orientations, and crack length on the critical stress intensity factors are discussed in detail. The results show that the special rotational deformation and the relative shear modulus of the upper the lower half plane have great effect on the lattice dislocation emission from the interface collinear crack tip.

1 Introduction

Nanocrystalline (nc) materials have been widely used in various fields because of their outstanding mechanical and physical performance, such as superior hardness, strength, and good wear resistance. But their low tensile ductility and low fracture toughness considerably limit their practical utility [1–20]. Nevertheless, some experimental studies have been performed for nc materials with the face-centered cubic (FCC) lattice, and it found that the nc materials show a ductile-to-brittle transition with decreasing grain size, which is not the same as in conventional coarse grain materials. Some other experiments display that several nc materials show considerable tensile ductility at room temperature and super plasticity at elevated temperature. The difference of nc materials lies in their certain special toughening mechanism caused by different structural features. Recently, some specific deformation mechanism has been developed to explain the specific toughening mechanism in nc materials, such as grain rotation, gain boundary sliding and migration, nanoscale deformation twinning, diffusion-assisted creep, and shear banding [21–28].

Recently, much attention has been paid to the rotational deformation, especially the special rotational deformation. It is formed in nanograin due to the formation of immobile wedge disclination quadrupole

M. Yu (✉)
College of Civil Engineering and Mechanics, Central South University of Forestry and Technology, Changsha 410004, China
E-mail: yumin1999@163.com

M. Yu
Hunan Province Key Laboratory of Engineering Rheology, Central South University of Forestry and Technology, Changsha 410004, China

Q. H. Fang · H. Feng · Y. W. Liu
State Key Laboratory of Advanced Design and Manufacturing for Vehicle Body, Hunan University, Changsha 410082, China

at nanograin boundary junctions, and the strengths of the immobile wedge disclinations gradually increase during their formation process conducted by grain boundary sliding and diffusion, and a wedge disclination that characterized by disclination strength represents a rotational line defect located at either a grain boundary or a triple junction of gain boundaries.

Many researches are focussed on the contribution of special rotational deformation to the fracture toughness of nc materials. In general, there will inevitably be various defects in nc materials, such as dislocations, cracks, inclusions, and nanoholes. For nc solids with cracks, the experimental studies and theoretical derivations have found that cracks can induce plastic shear by emission of lattice dislocations from crack tips as long as the stress intensity factor of crack tips is large enough, thus hindering cracks growth and improving the toughness of nc solids. So it is very meaningful to study the effects of special rotational deformation on the emission of lattice dislocations from various crack tips [29–37]. Our group has theoretically investigated the effect of special rotational deformation on the lattice dislocation emission from a line crack, a semi-elliptical blunt crack tip, and an elliptical hole in nc materials and has obtained a series of important conclusions. In this work, we are dedicated to quantitatively investigate the effect of special rotational deformation on the lattice dislocation emission from an interface collinear crack tip in nc bi-materials.

2 Problem formulations

The problem to be considered is shown in Fig. 1. A deformed nc bi-material solid contains a series of interfacial collinear cracks under remote model I and mode II loadings. The solid consists of nanoscale grains divided by lots of grain boundaries and is supposed to be elastically isotropic. The cracks are considered as flat and plane and the same along the coordinate axis z perpendicular to the xy plane, so the considered problem can be simplified to a two-dimensional model, which can definitely reflect the key of the problem.

For the plane strain problem, stress fields $(\sigma_{xx}, \sigma_{yy}, \sigma_{xy})$ and displacement fields (u_x, u_y) can be expressed in terms of two Muskhelishvili' complex potentials [38,39]:

$$\sigma_{xx} + \sigma_{yy} = 2\left[\Phi(z) + \overline{\Phi(z)}\right], \tag{1}$$

$$\sigma_{yy} - \mathrm{i}\sigma_{xy} = \Phi(z) + \overline{\Phi(z)} + z\overline{\Phi'(z)} + \overline{\Psi(z)}, \tag{2}$$

$$2\mu\left(u'_x + u'_y\right) = (3 - 4\upsilon)\,\Phi(z) - \overline{\Phi(z)} - z\overline{\Phi'(z)} - \Psi(z), \tag{3}$$

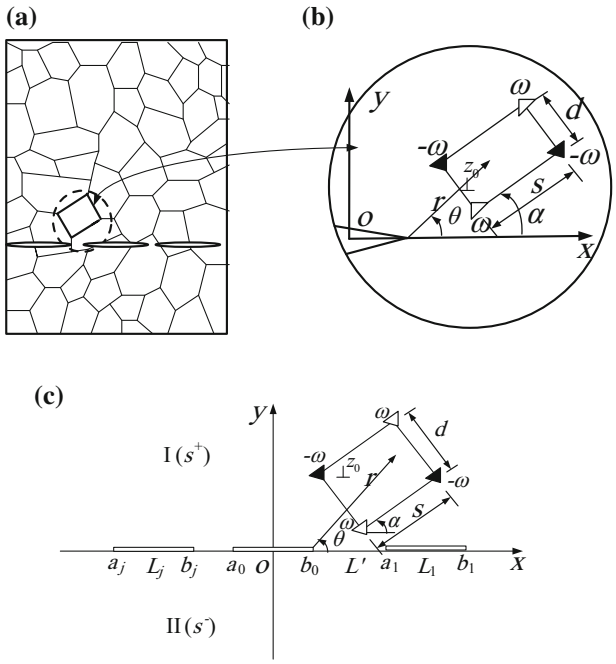

Fig. 1 The special rotational deformation in a plastic deformed nc bi-material containing collinear cracks and the dislocation emission from an interfacial collinear crack tip. **a** Two-dimensional nc bi-material solid with interfacial collinear cracks. **b** The magnified inset. **c** Calculation model

where $z = x + iy$, $u'_x = \partial u_x/\partial x$, $u'_y = \partial u_y/\partial x$, $\Phi'(z) = \mathrm{d}[\Phi(z)]/\mathrm{d}z$, $i = \sqrt{-1}$, "—" represents the complex conjugate. So the stress components σ_{xx}, σ_{yy} and σ_{xy} can be written as

$$\left.\begin{aligned}\sigma_{xx} &= \mathrm{Re}[2\Phi(z) - \bar{z}\Phi'(z) - \Psi(z)]\\ \sigma_{yy} &= \mathrm{Re}[2\Phi(z) + \bar{z}\Phi'(z) + \Psi(z)]\\ \sigma_{xy} &= \mathrm{Im}[\bar{z}\Phi'(z) + \Psi(z)]\end{aligned}\right\} \tag{4}$$

In the xy-plane, medium I with elastic properties μ_1, ν_1, and medium II with μ_2, ν_2 occupy the upper half plane (s^+) and the lower half plane ($s-$), respectively. A series of traction free interfacial collinear cracks L_j ($j = 0, 1, 2, \ldots$) with the tips at points a_j, b_j lie along the interface (x-axis) between two materials, and L is the union of the crack segments L_j while L' is the remainder of interface representing the complete connection part of the two kinds of material. The boundary conditions of the displacement and stress for the present problem can be expressed as follows [40]:

$$u^+_{x1}(t) + \mathrm{i}u^+_{y1}(t) = u^-_{x2}(t) + \mathrm{i}u^-_{y2}(t) \quad t \in L', \tag{5}$$

$$\sigma^+_{yy1}(t) - \mathrm{i}\sigma^+_{xy1}(t) = \sigma^-_{yy2}(t) - \mathrm{i}\sigma^-_{xy2}(t) \quad t \in L', \tag{6}$$

$$\sigma^+_{yy1}(t) - \mathrm{i}\sigma^+_{xy1}(t) = 0 \quad t \in L, \tag{7}$$

$$\sigma^-_{yy2}(t) - \mathrm{i}\sigma^-_{xy2}(t) = 0 \quad t \in L, \tag{8}$$

where the subscripts 1 and 2 denote the region s^+ and s^-, the superscripts + and − represent the boundary values of the physical quantity as z approaches the interface from s^+ and s^-, respectively.

Introducing a polar system (r, θ) with the origin at the right endpoint of the crack L_0, as shown in Fig. 1b. A disclination quadrupole, representing the special rotational deformation of a grain, appears near the crack tip in the upper half plane due to high stress concentration at the crack tip. It consists of two positive disclinations with strength ω at $z_1 = b_0 + r_1\mathrm{e}^{\mathrm{i}\theta_1}$ and $z_3 = z_1 + s\mathrm{e}^{\mathrm{i}\alpha} + d\mathrm{e}^{\mathrm{i}(\alpha+\pi/2)}$, and two negative disclinations with strength $-\omega$ at $z_2 = z_1 + s\mathrm{e}^{\mathrm{i}\alpha}$ and $z_4 = z_1 + d\mathrm{e}^{\mathrm{i}(\alpha+\pi/2)}$ in the medium I, respectively. Here s and d are the quadrupole arms, namely the grain size, α is the special rotational deformation orientation representing the angle between the crack plane and one of the quadrupole arms s.

For the problem shown in Fig. 1c, the complex potentials $\Phi^\omega_1(z)$ and $\Psi^\omega_1(z)$ in the medium I can be written as [41–45]

$$\Phi^\omega_1(z) = \Phi^\omega_{10}(z) + \Phi^\omega_{1*}(z) \quad z \in s^+, \tag{9}$$

$$\Psi^\omega_1(z) = \Psi^\omega_{10}(z) + \Psi^\omega_{1*}(z) \quad z \in s^+, \tag{10}$$

where the first items $\Phi^\omega_{10}(z)$ and $\Psi^\omega_{10}(z)$ denote that a wedge disclination quadrupole lies in the infinite upper plane with no crack embedded in, and the second items $\Phi^\omega_{1*}(z)$ and $\Psi^\omega_{1*}(z)$ represent the interaction between cracks and wedge disclination quadrupole, and they are holomorphic in the region $z \in s^+$. According to the work of Fang, we have [40]

$$\Phi^\omega_{10}(z) = \frac{D_1\omega}{2}\sum_{k=1}^{4}(-1)^{k+1}\ln(z - z_k) \quad z \in s^+, \tag{11}$$

$$\Psi^\omega_{10}(z) = -\frac{D_1\omega}{2}\sum_{k=1}^{4}(-1)^{k+1}\frac{\bar{z}_k}{z - z_k} \quad z \in s^+. \tag{12}$$

Here we only consider the typical case of a finite crack in interface, which may have some practical importance. Without loss of generality, we assume that the two ends of the crack are located at a_0 and b_0 on the interface. Adopting the results in the work of Fang and using the principle of superposition, the solutions to the interaction between a wedge disclination quadrupole in the upper half plane and a collinear interface crack can be obtained as [40,41]

$$\Phi^\omega_1(z) = \frac{D_1\omega}{2}\cdot\frac{1 - g + h}{1 - g}\sum_{k=1}^{4}(-1)^{k+1}\left[\ln\frac{z - z_k}{z - \bar{z}_k} - \frac{z - z_k}{z - \bar{z}_k}\right]$$

$$-\frac{D_1\omega}{2}\cdot\frac{hX_0(z)}{1-g}\cdot\sum_{k=1}^{4}(-1)^{k+1}$$
$$\left\{\frac{\ln(z-z_k)}{X_0(z_k)}+g(z_k-\bar{z}_k)-\frac{1}{X_0(\bar{z}_k)}\left[\frac{z-z_k}{z-\bar{z}_k}+\ln(z-\bar{z}_k)\right]\right\}, \tag{13}$$

$$\Phi_1^{\omega'}(z)=\frac{D_1\omega}{2}\cdot\frac{1-g+h}{1-g}\sum_{k=1}^{4}(-1)^{k+1}\left[\frac{1}{z-z_k}-\frac{2}{z-\bar{z}_k}+\frac{z-z_k}{(z-\bar{z}_k)^2}\right]$$
$$-\frac{D_1\omega}{2}\cdot\frac{hX_0'(z)}{1-g}\cdot\sum_{k=1}^{4}(-1)^{k+1}\left\{\frac{\ln(z-z_k)}{X_0(z_k)}+g(z_k-\bar{z}_k)-\frac{1}{X_0(\bar{z}_k)}\left[\frac{z-z_k}{z-\bar{z}_k}+\ln(z-\bar{z}_k)\right]\right\}$$
$$-\frac{D_1\omega}{2}\cdot\frac{hX_0(z)}{1-g}\sum_{k=1}^{4}(-1)^{k+1}\left\{\frac{1}{X_0(z_k)(z-z_k)}-\frac{1}{X_0(\bar{z}_k)}\left[\frac{2}{z-\bar{z}_k}-\frac{z-z_k}{(z-\bar{z}_k)^2}\right]\right\}, \tag{14}$$

$$\begin{aligned}\Psi_1^{\omega}(z)&=-\Phi_1^{\omega}(z)-z\bar{\Phi}_1^{\omega'}(z)-\bar{\Phi}_1^{\omega}(z)\\&=-\Phi_1^{\omega}(z)-z\bar{\Phi}_1^{\omega'}(z)-\frac{D_1\omega}{2}\cdot\frac{1-g+h}{1-g}\sum_{k=1}^{4}(-1)^{k+1}\left[\ln\frac{z-\bar{z}_k}{z-z_k}-\frac{z-\bar{z}_k}{z-z_k}\right]\\&\quad+\frac{D_1\omega}{2}\cdot\frac{h\overline{X_0}(z)}{1-g}\sum_{k=1}^{4}(-1)^{k+1}\left\{\frac{\ln(z-\bar{z}_k)}{\overline{X_0(z_k)}}+g(\bar{z}_k-z_k)-\frac{1}{\overline{X_0(\bar{z}_k)}}\left[\frac{z-\bar{z}_k}{z-z_k}+\ln(z-\bar{z}_k)\right]\right\},\end{aligned} \tag{15}$$

where $D_1=\frac{\mu_1}{2\pi(1-\nu_1)}$, $g=-\frac{\mu_2+\mu_1(3-4\nu_2)}{\mu_1+\mu_2(3-4\nu_1)}$, $h=-\frac{4\mu_2(1-\nu_1)}{\mu_1+\mu_2(3-4\nu_1)}$, $\beta=\frac{\ln|g|}{2\pi}$, $X_0'(z)=\frac{\mathrm{d}X_0(z)}{\mathrm{d}z}$, $X_0(z)=(z-a_0)^{-0.5-i\beta}(z-b_0)^{-0.5+i\beta}$.

3 Dislocation emission from the interfacial crack tip

Let us consider the emission of lattice dislocation from the interfacial crack tip. For simplicity, we just focus on the situation that the dislocation is of edge character and their Burgers vectors lie along the slip plane making an angle θ_0 with x-axis. The first edge dislocation is located at $z_0=b_0+r_0\mathrm{e}^{\mathrm{i}\theta_0}$ in the medium I and its Burgers vector is set as $b=b_x-ib_y$. Referring to the work of Ref. [39], the elastic fields of edge dislocation can be calculated by the following complex potentials $\Phi_1^e(z)$ and $\Psi_1^e(z)$:

$$\Phi_1^e(z)=\Phi_{10}^e(z)+\Phi_{1*}^e(z)\quad z\in s^+, \tag{16}$$
$$\Psi_1^e(z)=\Psi_{10}^e(z)+\Psi_{1*}^e(z)\quad z\in s^+, \tag{17}$$

where $\Phi_{10}^e(z)=\frac{\gamma_1}{z-z_0}$, $\Psi_{10}^e(z)=\frac{\bar{\gamma}_1}{z-z_0}+\frac{\gamma_1\bar{z}_0}{(z-z_0)^2}$, $\gamma_1=\frac{\mu_1}{4\pi(1-\nu_1)}\left(b_y-\mathrm{i}b_x\right)$.

Without loss of generality, we just consider the typical case of the interface with a finite crack and assume that the two ends of the crack are located at a_0 and b_0 on the interface. The specific expressions of $\Phi_1^e(z)$ and $\Psi_1^e(z)$ can be written as

$$\Phi_1^e(z)=h_1\left[\frac{\gamma_1}{z-z_0}-\frac{\gamma_1}{z-\bar{z}_0}-\frac{\bar{\gamma}_1(z_0-\bar{z}_0)}{(z-\bar{z}_0)^2}\right]+h_2\frac{X_0(z)}{X_0(z_0)}\frac{\gamma_1}{z-z_0}+h_2(1-g)\gamma_1X_0(z)$$
$$+h_2\frac{X_0(z)}{X_0(\bar{z}_0)}\left[\frac{\gamma_1}{z-\bar{z}_0}-\frac{\bar{\gamma}_1(\bar{z}_0-z_0)}{(z-\bar{z}_0)^2}-\frac{\bar{z}_0-\frac{1}{2}(a_0+b_0)+i\beta(a_0-b_0)}{(\bar{z}_0-a)(\bar{z}_0-b)}\frac{\bar{\gamma}_1(\bar{z}_0-z_0)}{(z-\bar{z}_0)}\right], \tag{18}$$

$$\Phi_1^{e'}(z)=h_1\left[-\frac{\gamma_1}{(z-z_0)^2}+\frac{\gamma_1}{(z-\bar{z}_0)^2}+\frac{2\bar{\gamma}_1(z_0-\bar{z}_0)}{(z-\bar{z}_0)^3}\right]+h_2\frac{X_0'(z)}{X_0(z_0)}\frac{\gamma_1}{z-z_0}-h_2\frac{X_0(z)}{X_0(z_0)}\frac{\gamma_1}{(z-z_0)^2}$$
$$+h_2\frac{X_0'(z)}{X_0(\bar{z}_0)}\left[\frac{\gamma_1}{z-\bar{z}_0}-\frac{\bar{\gamma}_1(\bar{z}_0-z_0)}{(z-\bar{z}_0)^2}-\frac{\bar{z}_0-\frac{1}{2}(a_0+b_0)+i\beta(a_0-b_0)}{(\bar{z}_0-a)(\bar{z}_0-b)}\frac{\bar{\gamma}_1(\bar{z}_0-z_0)}{(z-\bar{z}_0)}\right]$$

$$+h_2(1-g)\gamma_1 X_0'(z)$$
$$+h_2\frac{X_0(z)}{X_0(\bar{z}_0)}\left[-\frac{\gamma_1}{(z-z_0)^2}+\frac{2\bar{\gamma}_1(\bar{z}_0-z_0)}{(z-\bar{z}_0)^3}+\frac{\bar{z}_0-\frac{1}{2}(a_0+b_0)+i\beta(a_0-b_0)}{(\bar{z}_0-a)(\bar{z}_0-b)}\frac{\bar{\gamma}_1(\bar{z}_0-z_0)}{(z-\bar{z}_0)^2}\right], \tag{19}$$

$$\begin{aligned}\Psi_1^e(z)&=-\Phi_1^e(z)-z\bar{\Phi}_1^{e'}(z)-\bar{\Phi}_1^e(z)\\&=-\Phi_1^e(z)-z\bar{\Phi}_1^{e'}(z)+h_1\left[\frac{\bar{\gamma}_1}{z-\bar{z}_0}-\frac{\bar{\gamma}_1}{z-z_0}-\frac{\gamma_1(\bar{z}_0-z_0)}{(z-z_0)^2}\right]\\&\quad+h_2\frac{\overline{X_0}(z)}{\overline{X_0}(z_0)}\frac{\bar{\gamma}_1}{z-\bar{z}_0}+h_2(1-g)\gamma_1\overline{X_0}(z)\\&\quad+h_2\frac{\overline{X_0}(z)}{\overline{X_0}(\bar{z}_0)}\left[\frac{\bar{\gamma}_1}{z-z_0}-\frac{\gamma_1(z_0-\bar{z}_0)}{(z-z_0)^2}-\frac{z_0-\frac{1}{2}(a_0+b_0)-i\beta(a_0-b_0)}{(z_0-a)(z_0-b)}\frac{\gamma_1(z_0-\bar{z}_0)}{(z-z_0)}\right],\end{aligned} \tag{20}$$

where $h_1=\frac{4\mu_1(1-\nu_2)}{\mu_1(1-\nu_2)+\mu_2(1-\nu_1)}$, $h_2=\frac{4\mu_2(1-\nu_1)}{\mu_1(1-\nu_2)+\mu_2(1-\nu_1)}$.

The force acting on the edge dislocation consists of three parts: the image force, the force produced by the wedge disclination quadrupole, and the external force.

First, the image force can be obtained by using the Peach–Koehler formula as [43]

$$\begin{aligned}f_{\text{image}}=f_x^e-\mathrm{i}f_y^e&=\left[\widehat{\sigma}_{xy}b_x+\widehat{\sigma}_{yy}b_y\right]\\&\quad+\mathrm{i}\left[\widehat{\sigma}_{xx}b_x+\widehat{\sigma}_{xy}b_y\right]==\frac{\mu b^2}{4\pi(1-\nu_1)}\left(\frac{\Phi_e^*(z_0)+\overline{\Phi_e^*(z_0)}}{\gamma_1}+\frac{\bar{z}_0\Phi_e^{*'}(z_0)+\Psi_e^*(z_0)}{\bar{\gamma}_1}\right),\end{aligned} \tag{21}$$

where $\widehat{\sigma}_{xx}$, $\widehat{\sigma}_{yy}$, and $\widehat{\sigma}_{xy}$ are the components of the perturbation stress, and $\Phi_e^*(z_0)=\lim_{z\to z_0}\left[\Phi_1^e(z)-\Phi_{10}^e(z)\right]$, $\Phi_e^{*'}(z_0)=\lim_{z\to z_0}\frac{\mathrm{d}[\Phi_1^e(z)-\Phi_{10}^e(z)]}{\mathrm{d}z}$, $\Psi_e^*(z_0)=\lim_{z\to z_0}\left[\Psi_1^e(z)-\Psi_{e0}(z)\right]$.

Second, the force produced by wedge disclination quadrupole representing the special rotational deformation can be obtained as [43]

$$\begin{aligned}f_{\text{wedge}}=f_x^\omega-\mathrm{i}f_y^\omega&=\left[\sigma_{xy}(z_0)b_x+\sigma_{yy}(z_0)b_y\right]+\mathrm{i}\left[\sigma_{xx}(z_0)b_x+\sigma_{xy}(z_0)b_y\right]\\&=\frac{\mu b^2}{4\pi(1-\nu_1)}\left(\frac{\Phi_\omega(z_0)+\overline{\Phi_w(z_0)}}{\gamma_1}+\frac{\bar{z}_0\Phi_\omega'(z_0)+\Psi_\omega(z_0)}{\bar{\gamma}_1}\right),\end{aligned} \tag{22}$$

where σ_{xx}, σ_{yy}, and σ_{xy} are the components of the stress field produce by wedge disclination quadrupole representing the special rotational deformation.

Finally, the external force acting on the edge dislocation can be denoted as

$$f_\Gamma=b\sigma_{r\theta}, \tag{23}$$

where $r_{r\theta}$ is the in-plane stress due to the remote mode I and mode II stress intensity factors and $\sigma_{r\theta}=\left(\sigma_y-\sigma_x\right)\sin\theta\cos\theta+\sigma_{xy}\left(\cos^2\theta-\sin^2\theta\right)$.

For the linear elastic analysis of plane cases, conventional approaches have been soundly established by Muskhelishvili and Radok (1953) and Neuber (1985). On the basis of this analysis, Irwin obtained his well-known equations of the stress fields near a sharp crack, considering the first terms of series expansion. Then, the similar solutions to the present problem have been derived as [47]

$$\begin{Bmatrix}\sigma_x\\\sigma_y\\\sigma_{xy}\end{Bmatrix}=\frac{K_{\text{I app}}}{\sqrt{2\pi r}}\cos\frac{\theta}{2}\begin{Bmatrix}1-\sin\frac{\theta}{2}\sin\frac{3\theta}{2}\\1+\sin\frac{\theta}{2}\sin\frac{3\theta}{2}\\\sin\frac{\theta}{2}\cos\frac{3\theta}{2}\end{Bmatrix}+\frac{K_{\text{II app}}}{\sqrt{2\pi r}}\begin{Bmatrix}-\sin\frac{\theta}{2}\left(2+\cos\frac{\theta}{2}\cos\frac{3\theta}{2}\right)\\\sin\frac{\theta}{2}\cos\frac{\theta}{2}\cos\frac{3\theta}{2}\\\cos\frac{\theta}{2}\left(1-\sin\frac{\theta}{2}\sin\frac{3\theta}{2}\right)\end{Bmatrix}, \tag{24}$$

where $K_{\mathrm{I\ app}}$ and $K_{\mathrm{II\ app}}$ are the generalized mode I and mode II stress intensity factors produced by the remote loadings.

Then, Eq. (23) can be written as

$$f_\Gamma = b\sigma_{r\theta} = \frac{b}{\sqrt{2\pi r_0}}\left(l_1 K_{\mathrm{I\ app}} + l_2 K_{\mathrm{II\ app}}\right), \tag{25}$$

where $l_1 = \frac{1}{2}\sin\theta_0 \cos\frac{\theta_0}{2}$, $l_2 = \cos\frac{3\theta_0}{2} + \sin^2\frac{\theta_0}{2}\cos\frac{\theta_0}{2}$.

Thus, the force acting on the edge dislocation can be obtained as

$$f_{\mathrm{emit}} = f_x\cos\theta + f_y\sin\theta + f_\Gamma = \mathrm{Re}[f_{\mathrm{image}} + f_{\mathrm{wedge}}]\cos\theta - \mathrm{Im}\left[f_{\mathrm{image}} + f_{\mathrm{wedge}}\right]\sin\theta + f_\Gamma. \tag{26}$$

Substituting Eqs. (21), (22) and (25) into (26), we can get the expression of the dislocation emission force.

4 The critical stress intensity factors for the dislocation emission

We discuss the effects of the special rotational deformation on emission of lattice dislocations from crack tips. A commonly accepted criterion for emission of dislocations from a crack tip is that the force acting on them is equal to zero. Moreover, the dislocation distance to the crack surface must be equal to or larger than the dislocation core radius [48]. Combining Eqs. (21)–(26) and $f_{\mathrm{emit}} = 0$, the critical stress intensity factor K_{IC}^{app} and $K_{\mathrm{II}C}^{\mathrm{app}}$ for the dislocation emission can be calculated as follows:

$$K_{\mathrm{II}}^{\mathrm{app}} = 0, \quad K_{IC}^{\mathrm{app}} = \frac{\sqrt{2\pi r_0}}{bl_1}\left(\mathrm{Im}\left[f_{\mathrm{image}} + f_{\mathrm{wedge}}\right]\sin\theta - \mathrm{Re}\left[f_{\mathrm{image}} + f_{\mathrm{wedge}}\right]\cos\theta\right), \tag{27}$$

$$K_{\mathrm{I}}^{\mathrm{app}} = 0, \quad K_{\mathrm{II}C}^{\mathrm{app}} = \frac{\sqrt{2\pi r_0}}{bl_2}\left(\mathrm{Im}\left[f_{\mathrm{image}} + f_{\mathrm{wedge}}\right]\sin\theta - \mathrm{Re}\left[f_{\mathrm{image}} + f_{\mathrm{wedge}}\right]\cos\theta\right), \tag{28}$$

where $f_{\mathrm{image}} + f_{\mathrm{wedge}} = \frac{\mu b^2}{4\pi(1-\nu_1)}\left\{\frac{2\mathrm{Re}[\Phi_e^*(z_0)+\Phi_w(z_0)]}{\gamma_1} + \frac{\bar{z}_0\left[\Phi_e^{*\prime}(z_0)+\Phi_w'(z_0)\right]+[\Psi_e^*(z_0)+\Psi_w(z_0)]}{\bar{\gamma}_1}\right\}$.

5 Numerical analysis

The critical stress intensity factors $K_I C^{\mathrm{app}}$ and $K_{\mathrm{II}C}^{\mathrm{app}}$ for dislocation emission will be calculated by using Eqs. (27) and (28) in the situation where the special rotational deformation forms near the crack in medium I, as shown in Fig. 1. The critical stress intensity factors are normalized as $K_{IC}^0 = K_{IC}^{\mathrm{app}}/\mu_1\sqrt{b}$ and $K_{\mathrm{II}C}^0 = K_{\mathrm{II}C}^{\mathrm{app}}/\mu_1\sqrt{b}$, and the disclination strengths are set as $\pm\omega$. The special rotational deformation arms are defined as s and d, let $s = d$. The special rotational deformation orientation is assumed as α, and the dislocation position as $r_0 = b/2$. The quadrupole arms are supposed to be much smaller than the crack length l. The relative shear modulus is defined as $u = \mu_2/\mu_1$, and the nanocrystalline material is denoted as 3C-SiC, so $\mu_2 = 217\,\mathrm{GPa}$, $\nu_2 = 0.23$. Then, numerical examples of analysis are given to illustrate the effect of variable parameters on the critical stress intensity factors for dislocation emission.

Let us assume that $b = 0.25\,\mathrm{nm}$, $\alpha = \pi/6$, $r_1 = 0.15\,\mathrm{nm}$, $\theta_1 = \pi/36$, $\theta_0 = \pi/20$, $l = 2000\,\mathrm{nm}$, $d = 12\,\mathrm{nm}$. The variations of the normalized mode I critical stress intensity factor with disclination strength for different relative shear modulus are depicted in Fig. 2. It can be seen that, if $u < 1$, K_{IC}^0 increases with increasing disclination strength ω, and if $u \geq 1$, K_{IC}^0 decreases with increasing disclination strength ω. It is interested that K_{IC}^0 increases when the disclination strength is relatively big ($\omega = 5°$) and decreases when the disclination strength is relatively small ($\omega = 1°$) as the increment of the relative shear modulus u. It is obvious that the special rotational deformation will hinder the dislocation emission from interfacial crack tip if the upper half plane is relatively rigid, and promote the dislocation emission if the upper half plane is relatively soft.

Figure 3 depicts the variations of the normalized mode I critical stress intensity factor with relative shear model modulus for different disclination strengths when $\alpha = \pi/6$. $r_1 = 0.15\,\mathrm{nm}$, $\theta_1 = \pi/36$, $\theta_0 = \pi/20$, $l = 2000\,\mathrm{nm}$, $d = 12\,\mathrm{nm}$. K_{IC}^0 decreases with increasing relative shear modulus u when the special rotational deformation vanishes ($\omega = 0°$), and it is obvious that the dislocation can emit easily from a softer part around

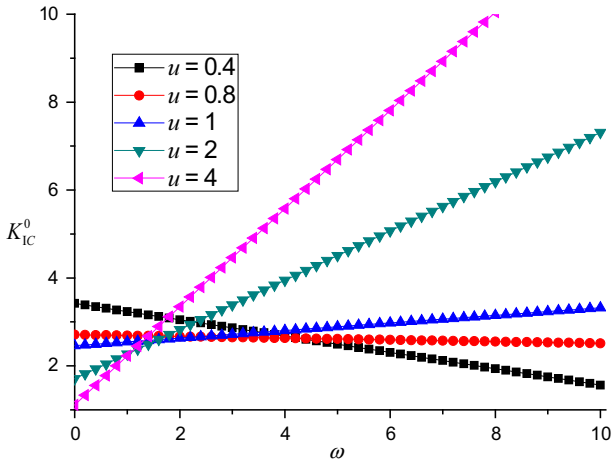

Fig. 2 Dependences of the critical normalized SIF K^0_{IC} on ω with different relative shear modulus u

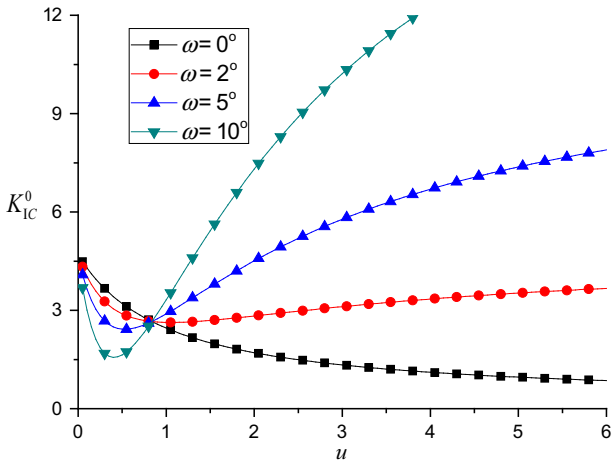

Fig. 3 Dependences of the critical normalized SIF K^0_{IC} on u with different disclination strengths ω

the interface crack. K^0_{IC} firstly increases and then decreases with increasing relative shear modulus u when the special rotational deformation occurs ($\omega \neq 0°$), so there exists an extreme of u_0 making the normalized mode I critical stress intensity factor a minimum value. The extreme of u_0 corresponds to the most probable relative shear modulus for dislocation emission. Moreover, K^0_{IC} decreases with increment of disclination strength when $u < 1$, while increases when $u > 1$, which agrees with the result in Fig. 2.

The variations of the critical normalized SIFs with the emission angel for different relative shear modulus are depicted in Fig. 4 when $\omega = 5°$, $\alpha = \pi/6$, $r_1 = 0.15\,\text{nm}$, $\theta_1 = \pi/36$, $l = 2000\,\text{nm}$, $d = 12\,\text{nm}$. For the mode I critical stress intensity factor in Fig. 4a, K^0_{IC} firstly decreases and then increases with increment of edge dislocation emission, so there exits an extreme of θ_e corresponding to the minimum value of K^0_{IC}, which indicates the most probable angle for dislocation emission. When u is specified as 0.4, 0.8, 1, 2, and 4, θ_e is equal to 36.5°, 28.5°, 27.1°, 26.9°, and 29.5°, respectively. It is obvious that θ_e increases with increasing the relative shear modulus when $u < 1$; however, it changes the opposite when $u > 1$. And when $u = 1$, meaning dislocation emitting from a sharp crack in a two-dimensional infinite nanograin, the variation laws are in accord with that in Ref. [41].

For model II critical stress intensity factor in Fig. 4b, K^0_{IIC} increases from a positive to infinity and then turns negative as the increasing of the dislocation emission angle. The sign of critical stress intensity factor is determined by the direction of Burgers vector of emitting dislocation. So the most probable emission angel for positive dislocation is always zero. In addition, the absolute value of the model II critical stress intensity factor increases with the relative shear modulus.

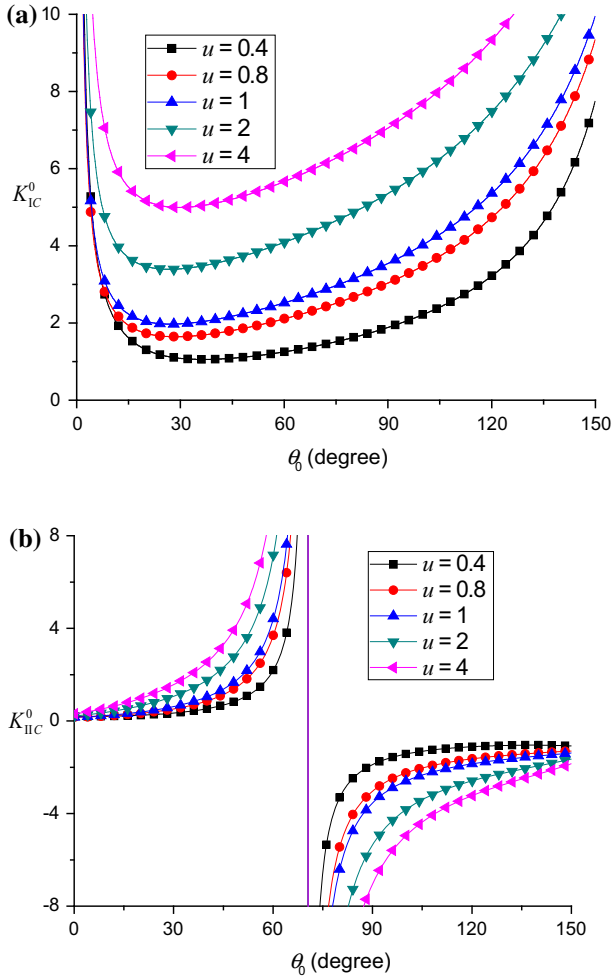

Fig. 4 Dependences of the critical normalized SIFs on the edge dislocation emission angle with different relative shear modulus for **a** K^0_{IC}; **b** K^0_{IIC}

Figure 5 depicts the dependences of the mode I critical normalized stress intensity factor K^0_{IC} on grain size with different relative shear modulus for $\omega = 5°$, $\alpha = \pi/6$, $r_1 = 0.15\,\text{nm}$, $\theta_1 = \pi/36$, $\theta_0 = \pi/20$, $l = 2000\,\text{nm}$. It can be seen that K^0_{IC} increases as the increment of relative shear modulus when the grain size is determined, which is in accord with the result in Figs. 2 and 3. When $u \geq 1$, K^0_{IC} first increases as the increment of the grain size and then decreases as the further increase in the grain size, so there is a minimum value named critical grain size corresponding to the maximum critical stress intensity factor, and K^0_{IC} reduces with increasing grain size when $u < 1$. It can also be seen that there is another critical grain size d_0 making $K^0_{IC} = 0$, so as long as $d > d_0$, dislocations can emit form interface crack tip without external load, and the critical grain size increases with increasing relative shear modulus, illustrating that when the upper half plane on which the dislocation is located is relatively soft, the critical grain size corresponding to dislocation emission become large.

Figure 6 plots the variations of K^0_{IC} with respect to the crack length for different relative shear modulus as $\omega = 5°$, $\alpha = \pi/6$, $r_1 = 0.15\,\text{nm}$, $\theta_1 = \pi/36$, $\theta_0 = \pi/20$, $d = 12\,\text{nm}$. It can be found that K^0_{IC} increases as the increment of crack length and K^0_{IC} also becomes larger as increasing relative shear modulus for certain crack length that is consistent with the previous conclusion.

In the following numerical analysis, taking the crack length as $l = 2000\,\text{nm}$, the upper plane and the lower plane of the materials are taken as the nanometer Ni and nanocrystal material 3C-SiC, so $\mu_1 = 73\,\text{GPa}$, $\nu_1 = 0.31$, $\mu_2 = 217\,\text{GPa}$, $\nu_2 = 0.23$ and the relative shear modulus $\mu = \frac{\mu_2}{\mu_1} \geq 1$.

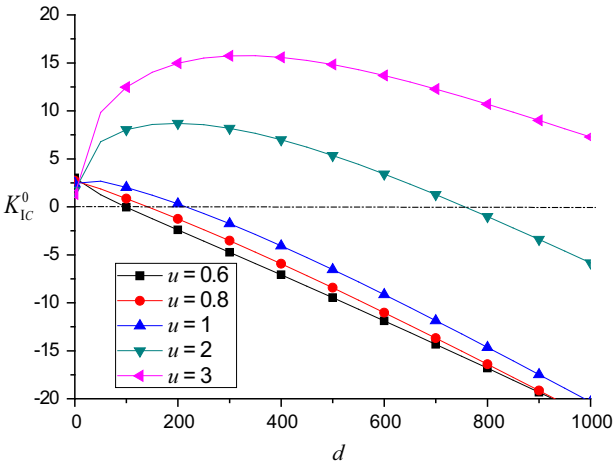

Fig. 5 Dependences of the critical normalized SIF K^0_{IC} on grain size with different relative shear modulus

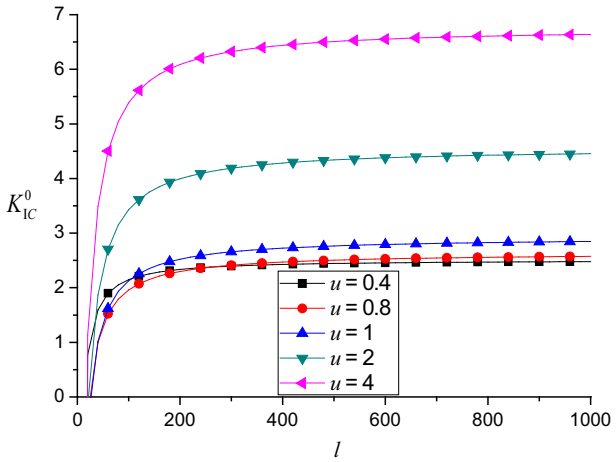

Fig. 6 Dependences of the critical normalized SIF K^0_{IC} on crack length with different relative shear modulus

The variations of critical normalized SIFs with disclination strength are shown in Fig. 7 when $\alpha = \pi/6$, $r_1 = 0.15\,\text{nm}$, $\theta_1 = \pi/36$, $\theta_0 = \pi/20$, $d = 12\,\text{nm}$. It is seen that K^0_{IC} and K^0_{IIC} both increase as the increment of disclination strength, and $K^0_{IIC} < K^0_{IC}$ for certain disclination strength, demonstrating that dislocations are more easily emitting under mode II loadings than mode I loadings. And K^0_{IC} and K^0_{IIC} get their own minimum value when $\omega = 0°$, which shows that the presence of special rotational deformation can hamper dislocation emitted from interfacial crack tip, thus reducing the toughness of material contributed by dislocation emission.

Figure 8 depicts the variations of critical normalized SIFs with the edge dislocation emission angle for different disclination strengths when $\alpha = \pi/6$, $r_1 = 0.15\text{nm}$, $\theta_1 = \pi/36$, $d = 12\,\text{nm}$. It can be seen that K^0_{IC} and $\left|K^0_{IIC}\right|$ increase with increasing disclination strength that consistent with the results in Fig.7 (here $u > 1$). K^0_{IC}first decreases as the increment of dislocation emission angle and then increases as the further increase in dislocation emission angle, so there is a most easily emission angle θ_e. When $\omega = 0°$, namely the special rotational deformation is not exist, the most easily emission angle is equal to 72.5°, which is the same as the result in Ref. [38]. And when the disclination strength is determined as 3°, 5°, 10°, θ_e is equals to 33°, 28.5°, 25.5°, respectively. So the most easily emission angle decreases as the increasing of disclination strength.

The variations of normalized SIF K^0_{IC} of the grain size d with different special rotational deformation orientations α are presented in Fig. 9 for $\omega = 5°, r_1 = 0.15\,\text{nm}, \theta_1 = \pi/36, \theta_0 = \pi/20$. The figure indicates the normalized SIF first increases then decreases with the increasing of the grain size d, so there will be a critical grain size making the critical normalized SIF equal to zero, and the critical grain size decreases as the increasing of α.

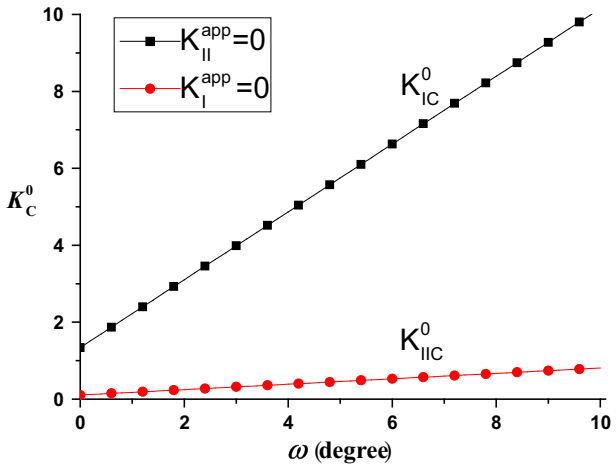

Fig. 7 Dependences of critical normalized SIFs on disclination strength

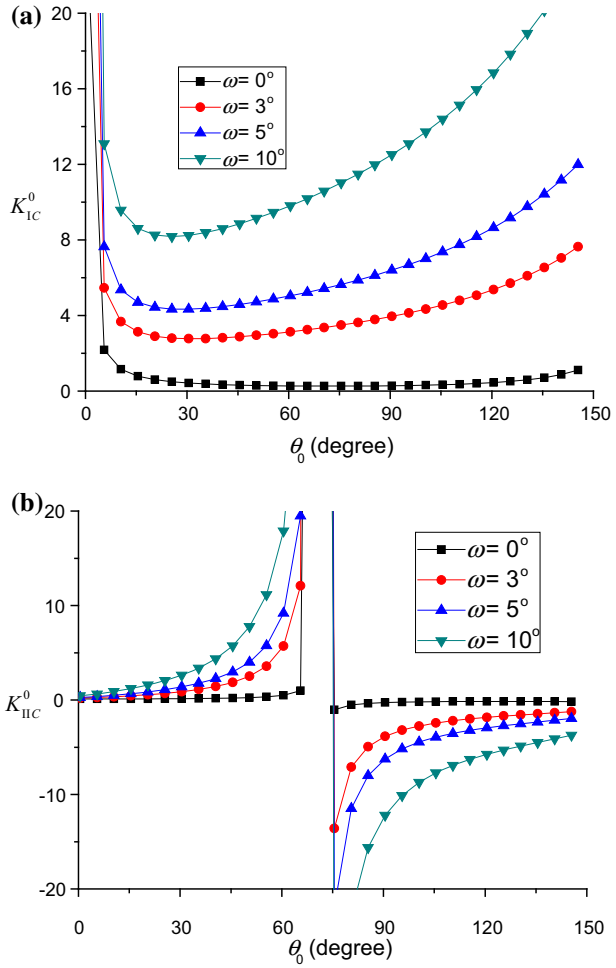

Fig. 8 Dependences of the critical normalized SIFs on the edge dislocation emission angle with different disclination strengths ω for **a** K_{IC}^{0}; **b** K_{IIC}^{0}

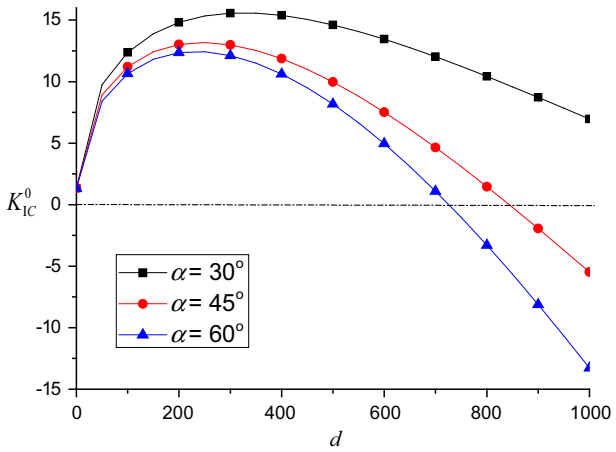

Fig. 9 Dependences of K_{IC}^0 on grain size d with different disclination quadrupole orientation angle α

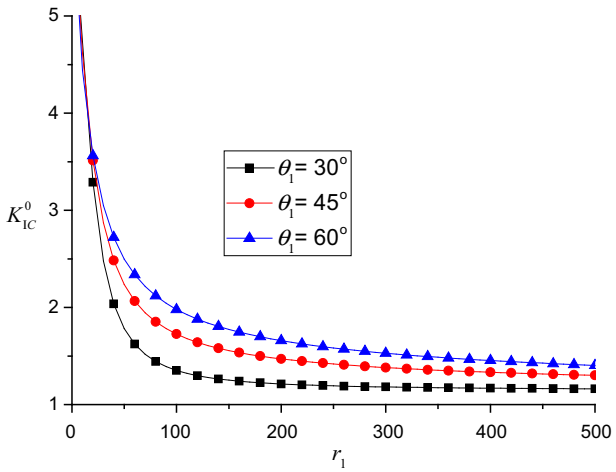

Fig. 10 Dependences of K_{IC}^0 on r_1 with different θ_1 ($\omega = 5°, \theta_0 = \pi/20, \alpha = \pi/6, d = 12$ nm)

The variations of normalized SIF K_{IC}^0 with the position of the first wedge disclination are depicted in Figs. 10 and 11. It can be seen that K_{IC}^0 decreases with increasing r_1 and finally tends to a constant when θ_1 is determined. K_{IC}^0 first decreases and then increases as the increasing of θ_1 when $r_1 = 0.1$ nm, but decreases as the the increasing of θ_1 when $r_1 = 0.5$ nm or 1 nm.

6 Conclusions

The effects of a disclination quadrupole produced by a nanograin's special rotational deformation on the emission of edge dislocations from a finite interfacial crack tip in a nanocrystalline bi-material solid are theoretically described using the complex variable method. The critical stress intensity factors for the first dislocation emission are given, and the influences of material properties, grain size, disclination strength, disclination location and orientation, special rotational deformation orientations, crack length on the critical stress intensity factors are discussed in detail. In summary, the following conclusions can be drawn:

1. The model I stress intensity factor increases as the increment of the relative shear modulus when the special rotational deformation does not exist, which shows that dislocations can easily emit form interface crack tips when the material is relatively soft. The model I stress intensity factor has its minimum corresponding to an extreme relative shear modulus u_0 that making dislocations the most easily emitted. So choosing appropriate materials of the upper plane and the lower plane can reduce the critical stress

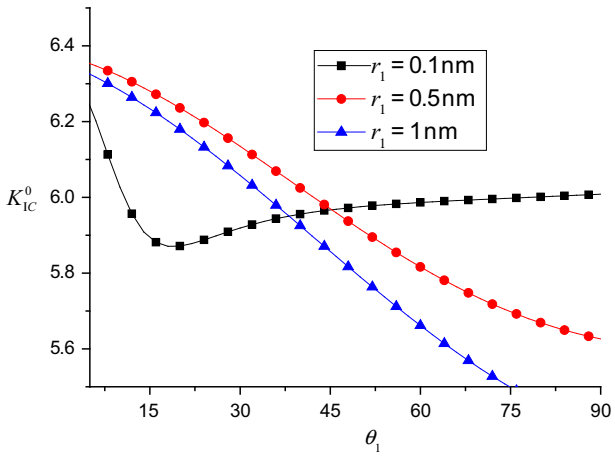

Fig. 11 Dependences of K_{IC}^0 on θ_1 with different r_1 ($\omega = 5°, \theta_0 = \pi/20, \alpha = \pi/6, d = 12$ nm)

intensity factor related to dislocation emission so as to facilitate a dislocation emission from the interface crack, thus improving the toughness of the nc bi-material.

2. The model II stress intensity factor is smaller than the model I stress intensity factor under the same disclination strength, showing that dislocations can move easily be emitted under model II loadings compared to model I loadings. And the critical stress intensity factors get their minimums when the special rotational deformation does not exist, and it is obvious that special rotational deformation will hinder dislocations emission from interfacial crack tips so as to reduced the toughness of materials caused by dislocation emission.
3. The model I critical stress intensity factor first decreases and then increases with increasing emission angle, so there is a minimum of the most probable emission angle. The most probable emission angle decreases with increasing relative shear modulus when $u < 1$, but increase when $u > 1$, and the most probable emission angle reduces as the increasing of disclination strength. The model II stress intensity factor may be negative or positive, which is determined by the direction of the Burgers vector of dislocations emitting from interface cracks. The most probable emission angel of positive edge dislocation is 0°, and the absolute value of critical stress intensity factors increases with increasing relative shear modulus.
4. There is an critical grain size making model I critical stress intensity factor equal to zero. As long as the grain size is larger than the critical value, dislocations can be emitted from the interfacial crack tip without external loads. The critical grain size increases with the increment of relative shear modulus and decreases with increasing dip angle of the disclination quadrupole arm, so when the upper plane of that dislocation is relatively soft, the grain size corresponding to dislocation emission becomes larger.

Acknowledgments The authors would like to deeply appreciate the support from the NNSFC (11572118, 11372103), the Hunan Provincial Science Fund for Distinguished Young Scholars (2015JJ1006). The work was also supported by the Introducing High-level Talent Research Fund of Central South University of Forestry and Technology (104-0096).

References

1. Zhu, L.L., Zheng, X.J.: Influence of interface energy and grain boundary on the elastic modulus of nanocrystalline material. Acta Mech. **213**(3), 223–234 (2010)
2. Liu, Y.G., Ju, R.Y.: A theoretical model for studying the mechanical properties of bimodal nanocrystalline materials. J. Mater. Res. **30**(11), 1836–1843 (2015)
3. Shen, L.M.: Combined grain size, strain rate and loading condition effects on mechanical behaviour of nanocrystalline Cu under high strain rates. Acta Mech Sin. **28**(4), 1125–1132 (2012)
4. Dao, M., Lu, L., Asaro, R.J., De Hosson, J.T.M., Ma, E.: Toward a quantitative understanding of mechanical behavior of nanocrystalline metals. Acta Mater. **55**, 4041–4065 (2007)
5. Wang, P., Yang, X.H., Tian, X.B.: Fracture behavior of precracked nanocrystalline materials with grain size gradients. J. Mater. Res. **30**(5), 709–716 (2015)
6. Meyers, M.A., Mishra, A., Benson, D.J.: Mechanical properties of nanocrystalline materials. Prog Mater Sci. **51**, 427–556 (2006)

7. Yu, M., Fang, Q.H., Feng, H., Liu, Y.W.: Effect of cooperative grain boundary sliding and migration on dislocation emitting from a semi-elliptical blunt crack tip in nanocrystalline solids. Acta Mech. **225**(7), 2005–2019 (2014)
8. Alizada, A.N., Sofiyev, A.H., Kuruoglu, N.: Stress analysis of a substrate coated by nanomaterials with vacancies subjected to uniform extension load. Acta Mech. **223**, 1371–1383 (2012)
9. Yu, M., Fang, Q.H., Feng, H., Liu, Y.W.: Effect of special rotational deformation on dislocation emission from a semi-elliptical blunt crack tip in nanocrystalline solids. J. Mater. Res. **28**(6), 798–805 (2013)
10. Zhou, K., Wu, M.S., Nazarov, A.A.: Relaxation of a disclinated tricrystalline nanowire. Acta Mater. **56**, 5828–5836 (2008)
11. Voyiadjis, George Z., Deliktas, Babur: Modeling of strengthening and softening in inelastic nanocrystalline materials with reference to the triple junction and grain boundaries using strain gradient plasticity. Acta Mech. **213**(1–2), 3–26 (2010)
12. Khan, A.S., Farrok, B., Takacs, L.: Effect of grain refinement on mechanical properties of ball-milled bulk aluminum. Mater. Sci. Eng. A **489**, 77–84 (2008)
13. Farrok, B., Khan, A.S.: Grain size, strain rate, and temperature dependence of flow stress in ultra-fine grained and nanocrystalline Cu and Al: synthesis, experiment, and constitutive modeling. Int. J. Plast. **25**(5), 715–732 (2009)
14. Aifantis, E.C.: Deformation and failure of bulk nanograined and UFG materials. Mater. Sci. Eng. A **530**, 190–201 (2009)
15. Barai, P., Weng, G.J.: Mechanics of very fine-grained nanocrystalline materials with contribution from grain interior, GB zone, and grain boundary sliding. Int. J. Plast. **25**, 2410–2434 (2009)
16. Xia, S.H., Wang, J.T.: A micromechanical model of toughening behavior in the dual-phase composite. Int. J. Plast. **26**, 1442–1460 (2010)
17. Barai, P., Weng, G.J.: Mechanics of a nanocrystalline coating and grain-size dependence of its plastic strength. Mech Mater. **43**, 496–504 (2011)
18. Liu, Y.G., Zhou, J.Q., Shen, T.D., Hui, D.: Effects of ultrafine nanograins on the fracture toughness of nanocrystalline materials. J. Mater. Res. **26**(14), 1734–1741 (2011)
19. Rupert, T.J., Trelewicz, J.R., Schuh, C.A.: Grain boundary relaxation strengthening of nanocrystalline Ni–W alloys. J. Mater. Res. **27**(9), 1285 (2012)
20. Liu, Y.G., Zhou, J.Q., Shen, T.D.: A combined dislocation-cohesive zone model for fracture in nanocrystalline materials. J. Mater. Res. **27**(4), 694–700 (2012)
21. KOvid'ko, I.A., Sheinerman, A.G.: Special strain hardening mechanism and nanocrack generation in nanocrystalline materials. Appl. Phys. Lett. **90**, 171927 (2007)
22. Cheng, S., Ma, E., Wang, Y.M., Kecskes, L.J., Youssef, K.M., Koch, C.C., et al.: Tensile properties of in situ consolidated nanocrystalline Cu. Acta Mater. **53**, 1521–1533 (2005)
23. Youssef, K.M., Scattergood, R.O., Murty, K.L., Horton, J.A., Koch, C.C.: Ultrahigh strength and high ductility of bulk nanocrystalline copper. Appl. Phys. Lett. **87**, 091904 (2005)
24. Youssef, K.M., Scattergood, R.O., Murty, K.L., Koch, C.C.: Nanocrystalline Al–Mg alloy with ultrahigh strength and good ductility. Scr. Mater. **54**, 251–256 (2006)
25. Sergueeva, A.V., Mara, N.A., Mukherjee, A.K.: Grain boundary sliding in nanomaterials at elevated temperatures. J. Mater. Sci. **4**, 1433–1438 (2007)
26. Liu, L.L., Zhang, Y.S., Zhang, T.Y.: Strain relaxation in heteroepitaxial films by misfit twinning: I. Critical thickness. J. Appl. Phys. **101**, 063501 (2007)
27. Zhang, Y.S., Liu, L.L., Zhang, T.Y.: Strain relaxation in heteroepitaxial films by misfit twinning: II. Equilibrium morphology. J. Appl. Phys. **101**, 063502 (2007)
28. Zhang, Y.S., Liu, L.L., Zhang, T.Y.: Critical thickness for misfit twinning in an epilayer. Int. J. Solids Struct. **45**, 3173–3191 (2008)
29. Zhao, Y., Qian, J., Daemen, L.L., Pantea, C., Zhang, J., Voroninm, G.A., et al.: Enhancement of fracture toughness in nanostructured diamond–SiC composites. Appl. Phys. Lett. **84**, 1356–1358 (2004)
30. Kaminskii, A.A., Akchurin, M.S., Gainutdinov, R.V., et al.: Microhardness and fracture toughness of Y_2O_3- and $Y_3Al_5O_{12}$-based nanocrystalline laser ceramics. Crystallogr. Rep. **50**, 569–573 (2005)
31. Bobylev, S.V., Morozov, N.F., Ovid'ko, I.A.: Cooperative grain boundary sliding and migration process in nanocrystalline solids. Phys. Rev. Lett. **105**, 055504 (2010)
32. Ovid'ko, I.A., Sheinerman, A.G., Aifantis, E.C.: Effect of cooperative grain boundary sliding and migration on crack growth in nanocrystalline solids. Acta Mater. **59**, 5023–5031 (2011)
33. Feng, H., Fang, Q.H., Zhang, L.C., Liu, Y.W.: Effect of cooperative grain boundary sliding and migration on emission of dislocations from a crack tip in nanocrystalline materials. Mech. Mater. **61**(15), 39–48 (2013)
34. Yu, M., Fang, Q.H., Liu, Y.W., Xie, C.: The interaction between a piezoelectric screw dislocation dipole and an elliptic blunt crack in elliptical inhomogeneity. Mech. Adv. Mater. Struct. **22**(5), 349–358 (2015)
35. Zhou, K.: Elastic field and effective moduli of periodic composites with arbitrary inhomogeneity distribution. Acta Mech. **223**(2), 293–308 (2012)
36. Xiao, Z.M., Chen, B.J.: A screw dislocation interacting with a coated fiber. Mech. Mater. **32**(8), 485–494 (2000)
37. Zhao, Y.X., Zeng, X., Chen, C.P.: Elastic behavior of disclination dipole near nanotube with surface/interface effect. Chin. Phys. B. **23**(3), 030202 (2014)
38. Muskhelishvili, N.L.: Some Basic Problems of Mathematical Theory of Elasticity. Noordhoff, Leyden (1975)
39. Zhang, T.Y., Li, J.C.M.: Interaction of an edge dislocation with an interfacial crack. J. Appl. Phys. **72**, 2215–2226 (1992)
40. Fang, Q.H., Liu, Y.W., Jiang, C.P., Li, B.: Interaction of a wedge disclination dipole with interfacial cracks. Eng. Fract. Mech. **73**, 1235–1248 (2006)
41. Fang, Q.H., Feng, H., Liu, Y.W., Lin, S., Zhang, N.: Special rotational deformation effect on the emission of dislocations from a crack tip in deformed nanocrystalline solids. Int. J. Solids Struct. **11–12**, 1406–1412 (2012)
42. Yu, M., Fang, Q.H., Liu, Y.W., Xie, C.: The interaction between a piezoelectric screw dislocation dipole and an elliptic blunt crack in elliptical inhomogeneity. Mech. Adv. Mater. Struct. **22**(5), 349–358 (2015)
43. Zhou, K., Wu, M.S.: Elastic fields due to an edge dislocation in an isotropic film-substrate by the image method. Acta Mech. **211**(3–4), 271–292 (2010)

44. Zhao, Y.X., Fang, Q.H., Liu, Y.W.: Effect of nanograin boundary sliding on nanovoid growth by dislocation shear loop emission in nanocrystalline materials. Eur. J. Mech-A/Solids **49**, 419–429 (2015)
45. Zhao, Y.X., Fang, Q.H., Liu, Y.W.: Effect of cooperative nanograin boundary sliding and migration on dislocation emission from a blunt nanocrack tip in nanocrystalline materials. Philos. Mag. **94**(7), 700–730 (2014)
46. Hirth, J.P., Lothe, J.: Theory of Dislocations, 2nd edn. Wiley, New York (1964)
47. Creager, M., Paris, P.C.: Elastic field equations for blunt cracks with reference to stress corrosion cracking. Int. J. Fract. **3**, 247–252 (1967)
48. Rice, J.R., Thomson, R.: Ductile versus brittle behavior of crystals. Philos. Mag. **29**, 73–80 (1974)